



**HAL**  
open science

# Investigation of hydrodynamics in high solid anaerobic digestion by particle image velocimetry and computational fluid dynamics: Role of mixing on flow field and dead zone reduction

Yuying Hu, Xiaohuan Zheng, Shihao Zhang, Wenjie Ye, Jing Wu, Souhila Poncin, Huai-Zhi Li

## ► To cite this version:

Yuying Hu, Xiaohuan Zheng, Shihao Zhang, Wenjie Ye, Jing Wu, et al.. Investigation of hydrodynamics in high solid anaerobic digestion by particle image velocimetry and computational fluid dynamics: Role of mixing on flow field and dead zone reduction. *Bioresource Technology*, 2021, 319, pp.124130. 10.1016/j.biortech.2020.124130 . hal-02946460

**HAL Id: hal-02946460**

**<https://hal.science/hal-02946460>**

Submitted on 23 Sep 2022

**HAL** is a multi-disciplinary open access archive for the deposit and dissemination of scientific research documents, whether they are published or not. The documents may come from teaching and research institutions in France or abroad, or from public or private research centers.

L'archive ouverte pluridisciplinaire **HAL**, est destinée au dépôt et à la diffusion de documents scientifiques de niveau recherche, publiés ou non, émanant des établissements d'enseignement et de recherche français ou étrangers, des laboratoires publics ou privés.



Distributed under a Creative Commons Attribution - NonCommercial 4.0 International License

1 **Investigation of hydrodynamics in high solid anaerobic**  
2 **digestion by particle image velocimetry and computational**  
3 **fluid dynamics: role of mixing on flow field and dead zone**  
4 **reduction**

5 Yuying Hu<sup>a,b,c</sup>, Xiaohuan Zheng<sup>a</sup>, Shihao Zhang<sup>a</sup>, Wenjie Ye<sup>a</sup>, Jing Wu<sup>b</sup>,  
6 Souhila Poncin<sup>c</sup>, Huai Z. Li<sup>c\*</sup>

7 *<sup>a</sup>School of Civil Engineering and Architecture, East China Jiao Tong University,*  
8 *Nanchang, 330013, China*

9 *<sup>b</sup>State Key Joint Laboratory of Environment Simulation and Pollution Control,*  
10 *School of Environment, Tsinghua University, Beijing, 100084, China*

11 *<sup>c</sup>Laboratory of Reactions and Process Engineering, Université de Lorraine, CNRS, 1,*  
12 *rue Grandville, BP 20451, 54001 Nancy cedex, France*

13

---

\*corresponding authors: Huai Z. Li

E-mail address: Huai-Zhi.Li@univ-lorraine.fr (H.Z. Li).

## 14 **Abstract:**

15 High solid anaerobic digestion (HSAD) was a potential organic waste treatment.  
16 Compared with low solid anaerobic digestion, it had the advantages of small footprint,  
17 less digestate, and low heating energy. However, HSAD's methane production is poor,  
18 mainly due to the complex hydrodynamics. In this study, computational fluid  
19 dynamics were utilized for HSAD's hydrodynamics investigation at 14.3% solid  
20 content and compared to the particle image velocimetry measurement. Then, effects  
21 of mixing on hydrodynamics were investigated. The results indicated that the  
22 diameter of impeller was critical for the radial mixing, and the distance between the  
23 impellers dictated the axial mixing. Besides, rotating speed affected flow velocities  
24 significantly, but displayed less effect on expanding the mixing range. Furthermore,  
25 HSAD's treating capacity could be increased at large extent by optimizing mixing.  
26 The visualization of the hydrodynamics in this study could potentially offer  
27 conceptual basis for HSAD's design in practical engineering.

28 **Keywords:** High solid anaerobic digestion, dead zone, hydrodynamic condition,  
29 computational fluid dynamics, particle image velocimetry.

## 30 **1. Introduction**

31 Anaerobic digestion could not only treat organic wastes but also recycle biogas <sup>[1,</sup>  
32 <sup>2]</sup>. Compared with other organic waste treatment technology (e.g. incineration and  
33 sanitary landfill), anaerobic digestion is more favorable from the environmental  
34 aspect which meets the demand for sustainable development<sup>[3]</sup>. High solid anaerobic  
35 digestion (HSAD), which is conducted at solid content higher than 10%, attracts  
36 extensive attention recently <sup>[1, 2, 4, 5]</sup>. It has the advantages of small footprint, less  
37 digestate, and low heating energy <sup>[6]</sup>. Decidedly, HSAD is the mainstream of  
38 anaerobic digestion in a near future <sup>[2, 4, 5]</sup>.

39 However, the flow pattern in HSAD is quite non-uniform and non-ideal <sup>[7]</sup>.  
40 HSAD's digestate is acknowledged as a highly viscous non-Newtonian fluid <sup>[8, 9]</sup> with  
41 the characteristics of shear-thinning, thixotropy and yield properties <sup>[7]</sup>. Incomplete  
42 mixing, short circuiting and the increment of inactive and stagnant zones usually  
43 occurred in HSAD system. These lead to the poor methane production and VS  
44 reduction of HSAD for the following reasons: (1) the poor hydrodynamics caused the  
45 accumulation of inhibition substrate like ammonia and volatile fatty acids (VFAs),  
46 which further lead to the ammonia or VFAs inhibition; (2) the inefficient mass and  
47 heat transfer also suppresses HSAD's performance<sup>[2, 10]</sup>. In this way, the better  
48 understanding of the complex hydraulics condition is crucial for HSAD's sufficient  
49 and stable operation. However, the relative reported investigation is still limited in  
50 this field.

51 Computational fluid dynamics (CFD) is a powerful tool which could be used for

52 the investigation of the flow pattern and mixing behavior in anaerobic digestion <sup>[11]</sup>.  
53 For example, CFD was used for the evaluation of flow field, turbulence intensity and  
54 mixing time in anaerobic co-digestion of chicken manure and food waste at 7% solid  
55 content <sup>[12]</sup>. Besides, the mixing quality in full scale biogas-mixed anaerobic digestion  
56 at 2.5% solid content was evaluated *via* CFD <sup>[11]</sup>. Azargoshasb <sup>[13]</sup> investigated the  
57 three phase hydrodynamics with the Eulerian multiphase approach and k - $\epsilon$  turbulence  
58 model (RNG) in a continuous stirred bioreactor. However, the work undertaken so far  
59 was usually focused on low solid anaerobic digestion with a solid content lower than  
60 10%. The application of CFD in HSAD is still quite limited for the major reason that  
61 the flow field of HSAD is difficultly measurable due to the lack of efficient measuring  
62 methods, and thus the CFD simulation is not able to be validated.

63 It is commonly recognized that the Particle Image Velocimetry (PIV) technique  
64 is an efficient tool for quantifying transparent flow fields. It could not only display the  
65 velocity distribution but also provide the quantitative information of the full flow field.  
66 The application of PIV in AD flow field has attracted increasing attention recently.  
67 Jiang et al. <sup>[14]</sup> has adopted the classical Metzner–Otto method for the mean shear rate,  
68 and PIV was used for the visualization of the instantaneous velocity field in the  
69 reactor at ss of 37 g SS/L. The unconfined gas mixing in anaerobic digestion was  
70 estimated by PIV in Dapelo’s study <sup>[15]</sup>. The present study mainly focused on the  
71 anaerobic digestion at low solid content. Such an application on HSAD was still rare  
72 to our best knowledge.

73 In our previous studies, novel insight was put towards the characteristics of  
74 HSAD’s flow fields *via* PIV <sup>[7]</sup>. It was noted that transparent 3.00% wet laponite  
75 suspension was introduced as the working model fluids for the similarity in both the  
76 rheological and structural characteristics. Though flow field visualization *via* PIV  
77 could help understand HSAD’s hydraulic condition, its application could only be  
78 conducted at lab scale. Thus, its guidance to practical engineering was not significant  
79 yet.

80 To conclude, the visualization of HSAD’s flow field *via* PIV is essentially  
81 limited at the lab-scale, and CFD lacks the validation methods. In this study, HSAD’s  
82 hydrodynamics was simulated by CFD and a comparison was performed with the PIV  
83 measuring results. The main advantages were as following: (1) the results were quite  
84 reliable because CFD results has been confirmed with the PIV measurements; (2)  
85 once validated at laboratory scale, the CFD approach could be applied to HSAD at  
86 different scales, including industrial size in practical applications. Besides, our  
87 previous finding revealed that the fluid around the impeller was mixed when only a  
88 single impeller was applied <sup>[7]</sup>. In this study, effects of both the impeller type and  
89 mixing speed on HSAD’s flow fields and dead zone are quantitatively evaluated. This  
90 study offers a potential access to the complex hydrodynamics in HSAD at practical  
91 engineering scale *via* CFD and PIV, and was essential for the stable and efficient  
92 performance of HSAD.

## 93 2. Materials and methods

### 94 2.1 Characteristics of HSAD digestate

95 In this study, HSAD digestate was taken from an HSAD reactor treating swine  
96 manure at lab-scale. Its total solid content was 14.3% and the volatile solid content  
97 was 11.3%. It was widely accepted that HSAD digestate was considered as  
98 non-Newtonian fluid at high solid content [11, 16]. The rheological characteristics of  
99 HSAD digestate was determined by a rheometer (AR-G2, TA, USA) in the shear  
100 rate of 0-10 s<sup>-1</sup>, and could be described as the power-law model [17]:

$$101 \quad \eta = K \dot{\gamma}^{n-1}$$

102 where  $\eta$  referred to the non-Newtonian fluid viscosity, Pa·s; K the consistency index,  
103 Pa·s<sup>n</sup>;  $\dot{\gamma}$  the shear rate, s<sup>-1</sup> and n the flow index. K and n were measured to be 52.8  
104 Pa·s<sup>n</sup> and 0.09 respectively.

### 105 2.2 Impeller pattern

106 In our previous study, only the fluid around the impeller could be mixed when  
107 HSAD was rotated with impeller of single stage<sup>[7]</sup>. Thus, in this study, different  
108 impeller diameter, impeller stages and the impeller types were taken into  
109 consideration to reveal their effects on flow field and dead zone distribution. The  
110 impellers were named as impeller A, impeller B and impeller C respectively. Besides,  
111 the mixing with impeller A, impeller B and impeller C were named as Case A, Case B  
112 and Case C respectively. The detailed description of the three impellers were as  
113 following:

114 (1) Impeller A was an impeller of double stages arranged abreast with the diameter of  
115 50 mm. The distance between the two impellers was 50mm, and the impeller height  
116 was 10 mm. It was comparable to our previous study<sup>[7]</sup> to reveal the effects of  
117 impeller's stages on axial flow.

118 (2) Impeller B was designed as impeller of three stages with the diameter of 90 mm,  
119 and was investigated for revealing impeller diameter's effects on flow pattern. The  
120 distance between the two impellers was 40 mm, and the impeller height was 10 mm.  
121 Besides, the effects of the distance between the impeller's stages on HSAD's flow  
122 field could also be evaluated.

123 (3) Impeller C was a ribbon impeller with the diameter of 90 mm. The impeller height  
124 was 140 mm. The relative study was used to reveal the effect of the impeller's type on  
125 the fluidity pattern.

## 126 **2.3 CFD simulation**

127 In this study, CFD simulation was performed *via* a commercial CFD software,  
128 ANSYS FLUENT 18.0. Considering that the HSAD digestate was non-Newtonian  
129 fluid of high viscosity and poor fluidity, the effect of produced biogas was limited on  
130 HSAD's hydrodynamics <sup>[12, 18-20]</sup>. In this way, the interaction between biogas and  
131 HSAD digestate was voluntarily neglected as suggested in the previous studies <sup>[12,</sup>  
132 <sup>18-20]</sup>. The geometry and mesh of both the reactor and impellers were generated using  
133 GAMBIT 2.4.6. The number of Case A, B and C grids were 312,696, 447,058,  
134 731,636 respectively. The minimum and maximum cell volume of each case were  
135 shown in Table 1. Afterwards, the obtained simulated results were compared with the  
136 PIV measured results to see whether they are reliable.

137 The flow and mixing facility could be assessed by the possible dead zone<sup>[9]</sup>, in  
138 which the velocity magnitude is below 0.001m/s<sup>[21]</sup>. Dead zone was considered  
139 stagnant and few mass transfer was taken place. In this way, the anaerobic digestion  
140 could be considered inefficient in such zone. In other words, the dead zone occupying  
141 reactor volume and consuming input energy contributes uselessly to the whole  
142 reaction and reactor's efficiency.

## 143 **2.4 Comparison with PIV measurements**

### 144 **2.4.1 Selection of the model fluid**

145 PIV could only be employed for the flow field measurements in transparent fluids,  
146 but sometimes the targeted fluid was opaque. Thus, the transparent model fluid was  
147 usually used to mimic real opaque fluids like blood<sup>[22]</sup>, cementitious composites<sup>[23]</sup>  
148 and so on. In our previous study, 3.00% (wt) laponite suspension was selected as the  
149 model fluid for their similarity in both rheological and structural properties compared  
150 to HSAD <sup>[7]</sup>. The rheological properties were measured by a rheometer (AR-G2, TA,  
151 USA) in the shear rate of 1 - 10 s<sup>-1</sup>. Besides, 3.00% (wt) laponite suspension was a  
152 structural colloid-liquid suspension, which is similar to the HSAD digestate. In this  
153 way, 3.00% (wt) laponite was chosen as the model fluid. The visualization of HSAD  
154 was only conducted at 14.3%.

### 155 **2.4.2 PIV measurement**

156

157 The detailed description of the experimental PIV technique could be found in our  
158 previous study<sup>[7]</sup>, and was summarized as follows. A transparent cylinder reactor  
159 which was continuously stirring with impeller A was filled with the model fluid (3.00%  
160 (wt) laponite suspension). The diameter and the height of the reactor was 100 mm and  
161 200 mm respectively. The height of the working fluid was 120 mm. In order to avoid  
162 the optical deformation due to the cylinder curvature, the reactor was placed in a  
163 transparent square vessel filled up with water whose refractive index (1.33) was the

164 same with that of 3.00% (wt) laponite suspension (1.33 [22]).

165 Afterwards, PIV measurements were conducted. The PIV instrument (Dantec  
166 Dynamics, Denmark) used in this study mainly composed of: a Dual Power 30-15  
167 Laser, a numerical CMOS camera, a central control unity and a computer.

168 The results of flow fields were computed through DynamicStudio software  
169 (Dantec Dynamics, Denmark). The produced flow fields were compared with the  
170 CFD simulation results to see whether they were reliable. If the CFD simulation was  
171 justified, the simulation was proved to be feasible and possibly extrapolated to  
172 installations of higher scale.

## 173 **2.5 Computations**

174 Generalized Reynolds number for non-Newtonian fluids was utilized for the  
175 characterization the flow pattern according to previous study<sup>[7, 23]</sup>:

$$176 \quad Re = \frac{\rho N^{2-n} D^2}{K} \quad (1)$$

177 where  $Re$  is the generalized Reynolds number,  $\rho$  is the density of the fluid,  $\text{kg}\cdot\text{m}^{-3}$ ,  $N$  is the  
178 rotation speed,  $\text{s}^{-1}$ ,  $D$  is the diameter of the impeller, m and  $K$  is the consistency,  $\text{Pa}\cdot\text{s}^n$ ;  $n$  is the  
179 flow index.

## 180 **3. Results and Discussion**

### 181 **3.1 Comparison of CFD simulation with PIV measurement**

182 In this study, our target was the investigation of HSAD's flow fields. PIV could  
183 only be employed for the flow field measurements in transparent fluids, but HSAD's  
184 digestate was opaque indeed. Thus, a model fluid, whose rheological and structural  
185 properties were similar to those of HSAD digestate, was utilized for PIV  
186 measurements to mimic HSAD's flow fields. As for the CFD approach, it was a  
187 numerical simulation technique which computed the flow fields based on the  
188 rheological properties of HSAD's digestate. In summary, the visualization of HSAD's  
189 flow field by PIV measurement in a model fluid could assess the reliability of CFD  
190 simulation before the extrapolation of CFD in real reactors involving other scales

191 The comparison of CFD simulation and PIV measurement (as mentioned in  
192 Section 2.4) was conducted in Case A at 100 rpm. The result of the CFD simulation  
193 was quite similar to that of PIV. Both of them revealed that the mixing region was  
194 only effective around the impeller, and the flow velocities around the impeller was  
195 around 0.1 m/s. However, there existed a difference that the flow field around the  
196 impeller measured by PIV was quite irregular compared with that of CFD modeling.  
197 This was closely related to the fact that PIV measurements were conducted with a  
198 model fluid and there existed some experimental fluctuations and noise, but CFD

199 simulation was an idealized numerical approach. To conclude, the CFD simulation  
200 was considered to be reliable. The visualization could potentially provide useful  
201 insight into the critical hydrodynamics for the practical engineering.

## 202 **3.2 Role of mixing**

### 203 **3.2.1 Visualization of Case A's hydrodynamics**

204 Flow fields in case A at different rotating speeds were graphically described in  
205 Fig. 1a. Obviously, the mixing region was just around the impeller at the low rotating  
206 speed of 50 rpm, 100 rpm, 150 rpm and 200 rpm. This phenomenon was quite similar  
207 to the experimental results measured by PIV in our previous study when only impeller  
208 of a single stage was used for mixing [7].

209 As the rotating speed continued to increase, it could be observed that the flow  
210 between the two impellers was strengthened gradually. In other words, compared with  
211 HSAD's flow field mixed with the impeller of a single stage observed in our previous  
212 study, increasing the number of impeller's stages was helpful to the mixing in the  
213 region between the impellers at high rotating speeds. Besides, it is worth noting that  
214 the flow near the axis was stagnant even at the rotating speed of 300 rpm.

215 Furthermore, the highest flow velocities occurred at the tip of the impeller, and was  
216 closely related to the fact that the tip speed was highest. Flow velocities was getting  
217 lower gradually from the tip due to the existence of HASD digestate's high viscosity.

218 Rotating speed could increase both the flow velocities and mixing range, but its  
219 efficiency on expanding HSAD's mixing range was limited. For example, sufficient  
220 mixing was achieved in the range of  $x = -25\text{mm} - 25\text{mm}$ ,  $y = 10\text{ mm} - 30\text{ mm}$ ,  $60$   
221  $\text{mm} - 80\text{mm}$  at rotating speed of 50 rpm, and it increased to  $x = -40\text{mm} - 40\text{mm}$ ,  $y =$   
222  $0\text{ mm} - 90\text{mm}$  when the rotating speed was increased to 300 rpm. Furthermore, the  
223 region ( $y = 90\text{ mm} - 150\text{ mm}$ ) could be difficultly mixed even at the rotating speed of  
224 300 rpm. In summarizing, both the radial and axial mixing was strengthened by  
225 increasing the rotating speed, however with a limited efficiency.

226 The spatial distribution of radial velocity at  $x = 20\text{ mm}$  was investigated. It could  
227 be observed that in the position near the impeller, the fluid was mixed vigorously with  
228 high velocities. The closer to the impeller the velocity was higher. Besides, the radial  
229 velocity at  $x = 20\text{ mm}$  increased with the rotating speed. Furthermore, it was  
230 interesting to note that the region between the impeller's stages was quiescent at low  
231 rotating speed (50 rpm), but became sufficiently mixed at high rotating speeds, e.g.  
232 rotating speed higher than 200 rpm. Furthermore, the region  $y > 90\text{ mm}$  was not  
233 mixed at all, even at the rotating speed of 300 rpm ( $\text{Re} = 2550$ ).

234 The axial velocity was evaluated at  $y = 20\text{ mm}$  and  $70\text{ mm}$ , referred to the central  
235 plane of the two impellers respectively. The axial velocity at these two planes was  
236 quite similar to each other, indicating that the mixing around the two stages was quite  
237 dependent in this case. Furthermore, the axial flow region expanded with the rotating  
238 speed. It was  $5\text{ mm} - 31\text{mm}$ ,  $5\text{ mm} - 38\text{mm}$ ,  $5\text{ mm} - 42\text{mm}$ ,  $5\text{ mm} - 47\text{mm}$  at 50,  
239 100, 150, 200, 250, 300 rpm respectively. Logically, the flow velocity increased with

240 the rotating speed too.

### 241 **3.2.2 Visualization of Case B's hydrodynamics**

242 The flow field in the HSAD reactor mixed by the impeller B was illustrated in  
243 Fig. 1b. Compared to Case A, Case B presented flow field with higher velocities at  
244 each corresponding rotating speed. This was closely related to the fact that the more  
245 impellers consumed more power at the same rotating speed. Thus, faster mixing was  
246 achieved in case B. Obviously, the mixing area was around the different stages of the  
247 impellers independently, and the mixing between the stages was not significantly  
248 enough at the rotating speed of 50 rpm. However, as the rotating speed further  
249 increased, the area between three stages was mixed gradually. This was quite different  
250 from the findings in case A where the area between the stages was only mixed at the  
251 rotating speed  $> 200$  rpm. These phenomena closely related to the distance between  
252 the two stages, i.e. the stages were closer and the area between them was easier to be  
253 mixed. In addition, both the flow velocities and mixing area were increased with the  
254 rotating speed. The radial mixing was achieved at each rotating speed, this proved  
255 again that the radial mixing was mainly determined by the diameter of the impeller at  
256 large extent rather than the rotating speed in such complex fluids, which corresponded  
257 to the observation in case A. Furthermore, the axial mixing was achieved in the range  
258 of  $y = 20$  mm – 140 mm at rotating speed of 50 rpm, and extended to 10 mm –150  
259 mm as the rotating speed increased to 300 rpm. Compared to the axial mixing in Case  
260 A (the range of  $y = 10$  mm – 90 mm), the axial mixing of  $y = 20$  mm – 140 mm in  
261 Case B seemed to confirm the role played by the stages of impeller. On the other side,  
262 similar to case A, flow velocities were highest at the tip of each impeller, and was  
263 gradually decreased to surrounding because of the high viscosity.

264 The radial velocities at  $x = 20$  mm were investigated. It could be observed that the  
265 radial velocities between the stages were about 0.02 m/s at 50 rpm. This was quite  
266 different from that in case A where the radial velocities between the stages were close  
267 to 0 m/s at 50 rpm. The difference between the two cases could arise from the distance  
268 between stages of the impellers: closer distance, easier flow driven. Furthermore, both  
269 the flow region and flow velocities increased with the rotating speed. On the other  
270 side, there were also some findings similar to Case A: the velocities near the impeller  
271 were higher and the radial velocities increased as the rotating speed increased.

272 The axial velocities at  $y = 40, 80, 120$  mm, referred to the central plane of the  
273 three impellers, were investigated. Unambiguously, the axial mixing around the three  
274 stages of the impeller was quite similar to each other. The axial mixing region was  
275 sufficient in this case, and depended on the diameter of the impeller. In addition, the  
276 axial velocities also increased with the rotating speed.

277

### 278 **3.2.3 Visualization of Case C's hydrodynamics**

279 The flow field in the HSAD induced by a ribbon impeller at different rotating  
280 speeds was presented in Fig.1c. It could be observed that the mixing was quite  
281 effective in the edge of the reactor, and then centralized gradually with the increasing  
282 rotating speed. This behavior was quite different from those in case A and case B

283 where the mixing was more efficient in the central part of the reactor than the edge.  
284 The radial mixing was achieved at  $x = -50 \text{ mm} - -30 \text{ mm}$  and  $x = 30 \text{ mm} - 50 \text{ mm}$  at  
285 the rotating speed of 50 rpm, but increased to  $x = -50 \text{ mm} - 50 \text{ mm}$  at the rotating  
286 speed of 300 rpm. The flow velocities increased with the rotating speed. Furthermore,  
287 the axial mixing was efficient even at the low rotating speed. It could be concluded  
288 that the ribbon impeller was more suitable for achieving the efficient mixing in HSAD  
289 compared to other impellers investigated here.

290 Furthermore, the spatial distribution of axial and radial velocities were quite  
291 complex. However, both axial and radial mixing was quite efficient in the whole  
292 reactor. For this reason, the ribbon impeller could achieve an efficient mixing even at  
293 low rotating speeds.

### 294 **3.3 Dead zone reduction**

295 The spatial distribution of dead zone in Case A could be found in Fig. 2a. The  
296 dead zone decreased with the rotating speed. It is worth noting that the region  
297 between the two stages of the impeller was a dead zone at the very beginning when  
298 the rotating speed was 50 rpm. However, the flow in this region was strengthened  
299 gradually as the rotating speed was increased, and the mixing in this zone became  
300 efficient at 300 rpm. Furthermore, it was worth noting that the zone in the upper  
301 section of the working fluid was dead zone even at the rotating speed of 300 rpm.

302 The ratio of the dead zone at different rotating speeds in Case A was shown in Fig.  
303 2b. It could be observed that dead zone comprised for quite large fraction in the  
304 HSAD reactor, and ranged between 65.2% – 90.5%. That is to say the efficient flow  
305 and mixing was only achieved in 9.5% – 34.8% active volume of the whole reactor.  
306 This indicated that the potential in increasing the treating capacity of HSAD was huge.  
307 In this regard, the inefficient mixing could be one of the major explanations for  
308 HSAD's poor methane production. Besides, increasing rotating speed of the impeller  
309 could decrease the ratio of dead zone to some extent, but the decrement was not  
310 sufficient. The dead zone ratio was in reverse linear relationship with rotating speed  
311 (50 – 300 rpm) with the  $R^2$  of 0.9871, and could be described as follows:

$$312 \quad y = -0.1x + 94.067 \quad (1)$$

313 where  $x$  was the rotating speed (rpm), and  $y$  was the volume ratio of dead zone (%).

314 As for the case B, the dead zone was quite limited in the reactor (Fig.2 a), i.e.  
315 dead zone only occupied in the edge and bottom of the reactor. It is worth noting that  
316 the zone between each impeller was active even at 50 rpm. In conclude, effective  
317 axial mixing could be achieved when the distance between the stages of impellers was  
318 close, and the radial mixing could be achieved when the diameter of the impeller is  
319 large enough.

320 The relationship between the dead zone and rotating speed in Case B was shown  
321 in Fig.2b. Compared to Case A, the dead zone ratio of case B was much lower (7.1% -  
322 18.4%). This was closely related the fact that the more impellers consumed logically  
323 more power at the same rotating speed. The effect of the rotating speed on the  
324 reduction of the dead zone in case B was much less obvious. Only 11.3% dead zone

325 was reduced when the rotating speed was increased from 50 to 300 rpm. This  
326 indicated that increasing rotating speed was not necessary for decreasing the dead  
327 zone ratio in HSAD.

328 The distribution of dead zone in Case C was presented in Fig.2a. At 50rpm, the  
329 dead zone in Case C was quite limited, only occupying the edge of the reactor. As the  
330 rotating speed continuing increased, the dead zone disappeared gradually.

331 The ratio of dead zone was quite small, typically around 4.4% – 5.9% when the  
332 rotating speed was 50 – 300 rpm. This indicated that the ribbon impeller could  
333 achieve efficient mixing even at 50 rpm. Furthermore, the increasing of rotating speed  
334 seemed to induce negligible effect on the reduction of the dead zone which was  
335 relatively stable at 50 – 300 rpm. Thus, the ribbon impeller could be considered  
336 suitable for HSAD's mixing.

337 The following observations can be drawn by comparing the mixing efficiency in  
338 each case:

339 (1) The mixing in Case A seemed to be poorest. The ratio of the dead zone could be as  
340 high as 90.5%, increasing rotating speed could strengthen the flow and mixing to  
341 some extent.

342 (2) The flow and mixing in Case B were more effective than Case A. The ratio of the  
343 dead zone ranged from 7.1% to 18.4%. The rotating speed played a negligible role in  
344 its reduction.

345 (3) In Case C, the mixing was quite efficient. The dead zone ratio was only 4.4% -  
346 5.9%. The rotating speed almost had no effect on the dead zone.

347 Among these three types of the impellers, the ribbon impeller was the most  
348 suitable for the HSAD mixing at any rotating speed (50 rpm – 300 rpm). However, the  
349 energy consumption of the ribbon impeller was too high to be applied in the practical  
350 engineering. In this way, multiple impellers arranged abreast was recommended for  
351 the HSAD. In particular, special attention should be paid to the impeller's diameter  
352 and the distance between stages.

### 353 **3.4 Practical implication and perspectives**

354 From the above-mentioned observations, it was beyond our expectation that the  
355 HSAD's dead zone ratio in each case displayed significant difference: the efficient  
356 active volume (total volume – dead zone) in Case A, Case B and Case C were 9.5 % –  
357 34.8%, 81.6% – 92.9% and 94.1% – 95.6% respectively. The proper selection of the  
358 mixing equipment could increase the treating capacity at large extent. Without any  
359 doubt, such a potential increment in treating capacity confirms the attraction of HSAD  
360 at large extent. In this way, the present study throws new insight to the flow pattern in  
361 an efficient AD system, especially at high solid content. It could also provide some  
362 fundamental information for the design and optimization of HSAD reactor.

363 In the future, the mixing consumption should also be evaluated. Proper mixing  
364 should be selected based on the power consumption, flow pattern and reactor  
365 performance. Besides, the effect of scale-up on the flow field of HSAD should also be  
366 quantified, for the reason that there existed some difference between the flow field in

367 the industrial and lab-scale HSAD systems.

## 368 **4. Conclusion**

369 The visualization of HSAD's flow fields was numerically simulated by the CFD  
370 approach, then compared with the experimental PIV results. The validated CFD  
371 approach could then be extended to real reactors involving different scales. Besides,  
372 the radial mixing of HSAD depended mainly on impeller's diameter, as well as the  
373 distance between stages. The effect of the rotating speed was significant on flow  
374 velocities, and contrariwise relatively limited on mixing range. The proper selection  
375 of the mixing equipment could possibly increase both the treating capacity and  
376 methane production. This could reinforce assuredly the attraction of HSAD in  
377 industrial applications.

### 378 **Acknowledgments:**

379 Financial support for this research was provided by the Natural Science Foundation of  
380 China (51908214), Primary Research & Development Plan of Jiangxi  
381 (20192BBH80009, 20202BAB213020), Science and technology research project of  
382 Jiangxi Provincial Department of Education (GJJ180298) and National Students'  
383 platform for innovation and entrepreneurship training program (201910404011).  
384 Supplementary data associated with this article can be found, in the online version.

### 385 **Notes:**

386 All authors declare no actual or potential conflict of interest.

## 387 **Reference**

- 388 [1] Y.Y. Hu, J. Wu, H.Z. Li, S. Poncin, K.J. Wang, J.E. Zuo. Study of an enhanced dry anaerobic digestion  
389 of swine manure: Performance and microbial community property[J]. *Bioresource Technology*,  
390 2019,282:353-360.
- 391 [2] W. Peng, F. Lü, L. Hao, H. Zhang, L. Shao, P. He. Digestate management for high-solid anaerobic  
392 digestion of organic wastes: A review[J]. *Bioresource Technology*, 2020,297:122485.
- 393 [3] X. Li, S. Chen, B. Dong, X. Dai. New insight into the effect of thermal hydrolysis on high solid sludge  
394 anaerobic digestion: Conversion pathway of volatile sulphur compounds[J]. *Chemosphere*,  
395 2020,244:125466.
- 396 [4] Y. Fan, Z. Lei, X. Yang, M. Kobayashi, Y. Adachi, Z. Zhang, K. Shimizu. Effect of nano-bubble water on  
397 high solid anaerobic digestion of pig manure: Focus on digestion stability, methanogenesis  
398 performance and related mechanisms[J]. *Bioresource Technology*, 2020,315:123793.
- 399 [5] H. Nam Joey Ting, L. Lin, R. Bello Cruz, B. Chowdhury, I. Karidio, H. Zaman, B. Ranjan Dhar.  
400 Transitions of microbial communities in the solid and liquid phases during high-solids anaerobic  
401 digestion of organic fraction of municipal solid waste[J]. *Bioresource Technology*, 2020:123951.

402 [6] H.-G. Guo, Q.-L. Chen, H.-W. Hu, J.-Z. He. High-solid anaerobic co-digestion of pig manure with  
403 lignite promotes methane production[J]. *Journal of Cleaner Production*, 2020,258:120695.

404 [7] Y. Hu, J. Wu, S. Poncin, Z. Cao, Z. Li, H.Z. Li. Flow field investigation of high solid anaerobic digestion  
405 by Particle Image Velocimetry (PIV)[J]. *Science of The Total Environment*, 2018,626:592-602.

406 [8] L. Yu, J. Ma, S. Chen. Numerical simulation of mechanical mixing in high solid anaerobic digester[J].  
407 *Bioresource Technology*, 2011,102(2):1012-1018.

408 [9] G. Leonzio. Study of mixing systems and geometric configurations for anaerobic digesters using  
409 CFD analysis[J]. *Renewable Energy*, 2018,123 578-589.

410 [10] Y.-y. Hu, C. Pan, X. Zheng, F. Hu, L. Xu, G. Xu, Y. Jian, X. Peng. Prediction and optimization of  
411 adsorption properties for Cs+on NiSiO@NiAlFe LDHs hollow spheres from aqueous solution: Kinetics,  
412 isotherms, and BBD model[J]. *Journal of Hazardous Materials*, 2020:123374.

413 [11] D. Dapelo, J. Bridgeman. Assessment of mixing quality in full-scale, biogas-mixed anaerobic  
414 digestion using CFD[J]. *Bioresource Technology*, 2018,265:480-489.

415 [12] L. Mao, J. Zhang, Y. Dai, Y.-W. Tong. Effects of mixing time on methane production from anaerobic  
416 co-digestion of food waste and chicken manure: Experimental studies and CFD analysis[J]. *Bioresource*  
417 *Technology*, 2019,294:122177.

418 [13] S.M.M. H. Azargoshab , T. Amani b, A. Jafari c, M. Nosrati Three-phase CFD simulation coupled  
419 with population balance equations of anaerobic syntrophic acidogenesis and methanogenesis  
420 reactions in a continuous stirred bioreactor[J]. *Journal of Industrial and Engineering Chemistry*,  
421 2015,27:207–217.

422 [14] J. Jiang, J. Wu, S. Poncin, H.Z. Li. Effect of hydrodynamic shear on biogas production and granule  
423 characteristics in a continuous stirred tank reactor[J]. *Process Biochemistry*, 2016,51(3):345-351.

424 [15] D. Dapelo, R. Trunk, M.J. Krause, J. Bridgeman. Towards Lattice-Boltzmann modelling of  
425 unconfined gas mixing in anaerobic digestion[J]. *Computers & Fluids*, 2019,180:11-21.

426 [16] J. Jiang, J. Wu, S. Poncin, H.Z. Li. Rheological characterization of digested sludge by solid sphere  
427 impact[J]. *Bioresource Technology*, 2016,218:301-306.

428 [17] M. Meister, M. Rezavand, C. Ebner, T. Pümpel, W. Rauch. Mixing non-Newtonian flows in  
429 anaerobic digesters by impellers and pumped recirculation[J]. *Advances in Engineering Software*,  
430 2018,115:194-203.

431 [18] Y. Zhang, G. Yu, L. Yu, M.A.H. Siddhu, M. Gao, A.A. Abdeltawab, S.S. Al-Deyab, X. Chen.  
432 Computational fluid dynamics study on mixing mode and power consumption in anaerobic mono- and  
433 co-digestion[J]. *Bioresource Technology*, 2016,203:166-172.

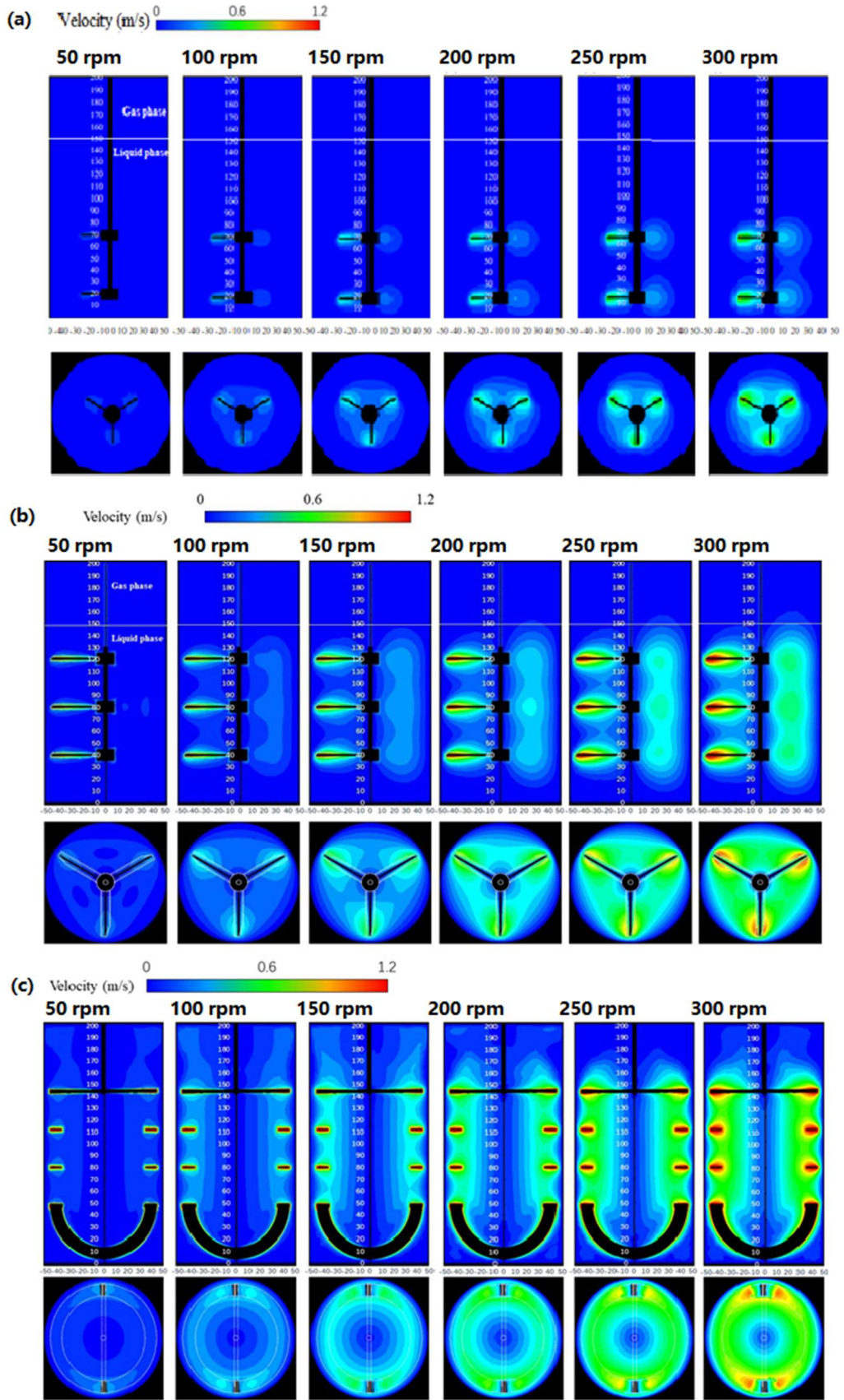
434 [19] J. Zhang, Q. Qi, L. Mao, Y. He, K.-C. Loh, Y. Wah Tong. Mixing strategies – Activated carbon nexus:  
435 Rapid start-up of thermophilic anaerobic digestion with the mesophilic anaerobic sludge as  
436 inoculum[J]. *Bioresource Technology*, 2020,310:123401.

437 [20] X. Zhai, I.D. Kariyama, B. Wu. Investigation of the effect of intermittent minimal mixing intensity  
438 on methane production during anaerobic digestion of dairy manure[J]. *Computers and Electronics in*  
439 *Agriculture*, 2018,155:121-129.

440 [21] B. Wu, S. Chen. CFD simulation of non-Newtonian fluid flow in anaerobic digesters[J].  
441 2008,99(3):700-711.

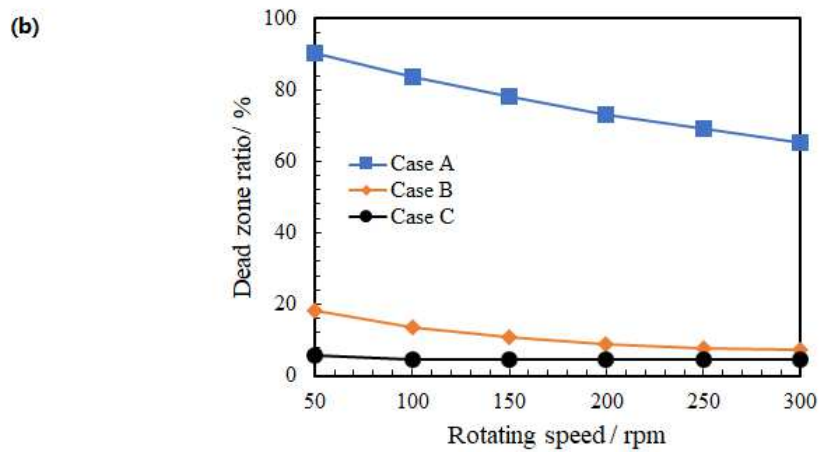
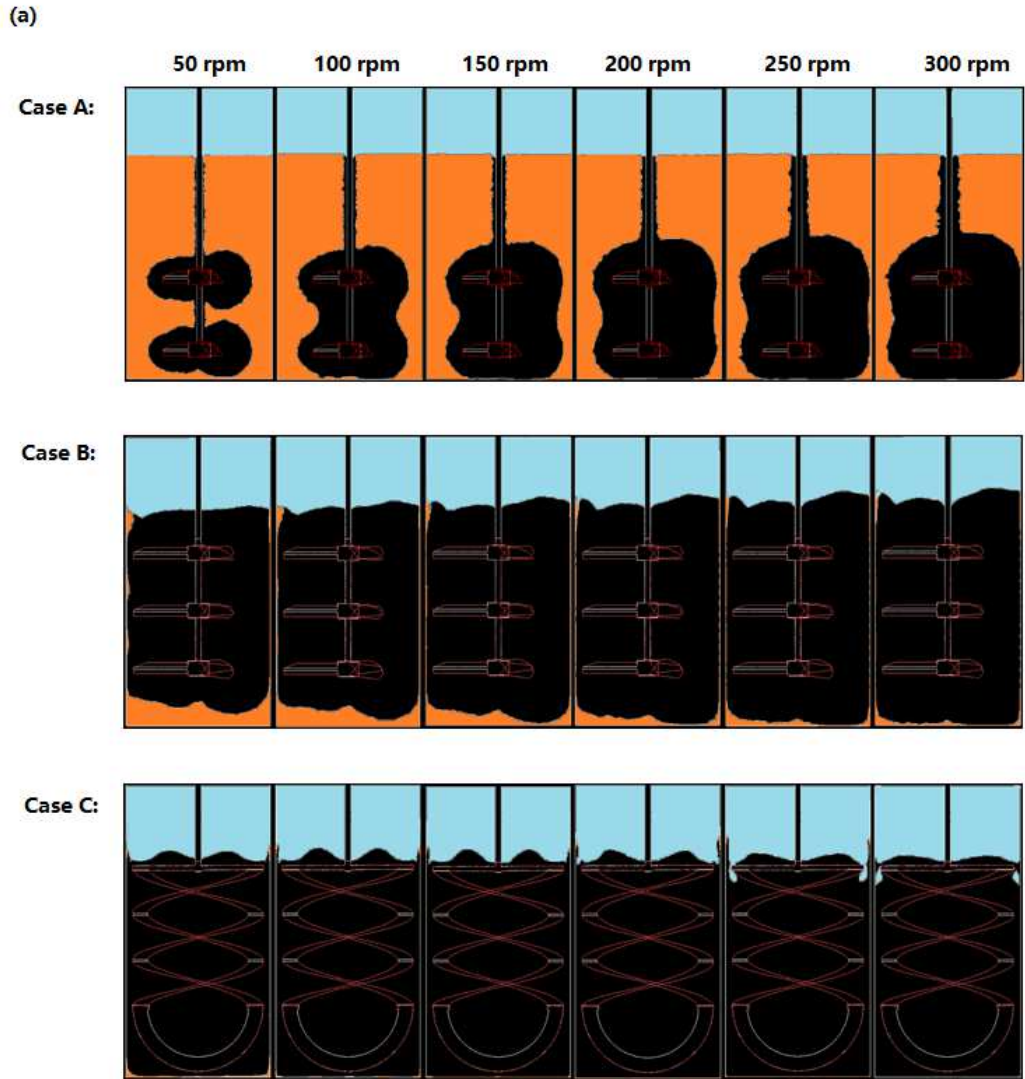
442 [22] Y.M. Nimdeo, Y.M. Joshi, K. Muralidhar. Refractive index measurement of sol forming Laponite JS  
443 dispersion using interferometry[J]. *Applied Clay Science*, 2016,123:272-278.

444 [23] N.M. Entsar. Mixing process of apple juice concentrate[J]. *Int. J. Nutr. Food Sci*, 2016(5):1-6.



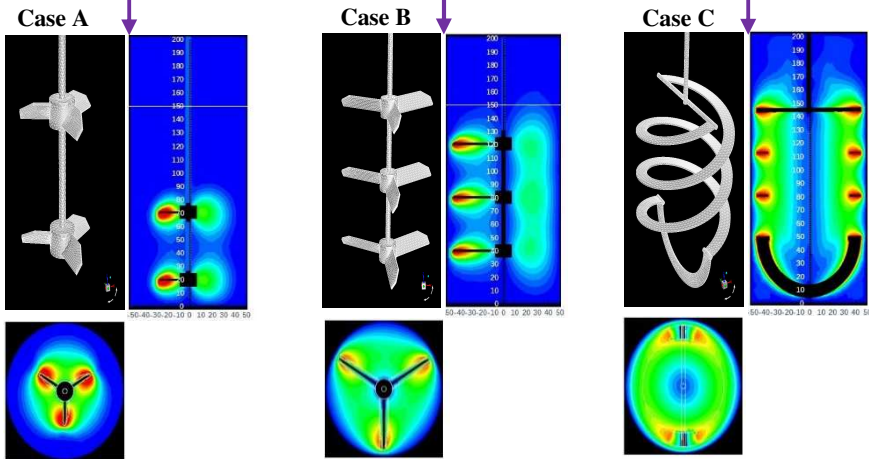
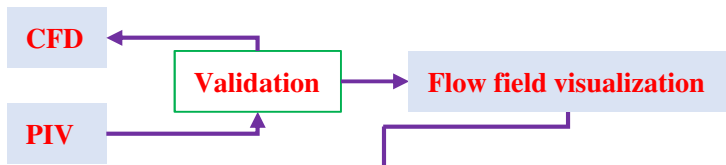
445  
446  
447

Fig. 1 Flow field at various rotating speeds of (a) Case A, (b) Case B and (c) Case C



448  
449  
450  
451  
452

**Fig.2** (a) Dead zone distribution in each cases at different rotating speed (the yellow section was the dead zone) and (b) dead zone ratio in each cases



**Dead zone ratio**

